Overconsolidation and Stiffness of Venice Lagoon Sands and Silts from SDMT and CPTU

Paola Monaco[1]; Sara Amoroso[2]; Silvano Marchetti[3]; Diego Marchetti[4]; Gianfranco Totani[5]; Simonetta Cola[6]; and Paolo Simonini[7]

Abstract: This study is part of an extensive research program carried out at the Treporti test site (Venice, Italy), where a cylindrical trial embankment was constructed and monitored from the beginning of its construction until complete removal, 4 years later. This paper concentrates mainly on the evaluation of overconsolidation and stiffness of the Venice lagoon sands and silts. The possibility of estimating the overconsolidation ratio (OCR) in sand by the combined use of seismic dilatometer (SDMT) tests and piezocone (CPTU) tests is investigated. A tentative correlation for estimating the OCR in sand from the ratio M_{DMT}/q_t is constructed. Field compression curves have been back-figured from 1-m field oedometer curves reconstructed from local vertical strains measured by a sliding deformeter under the embankment center. The SDMT and CPTU soundings performed before embankment application and postremoval have permitted analyzing how the OCR caused by the embankment was reflected by the before/after SDMT and CPTU results. The paper also illustrates the possible use of the SDMT to assess the in situ decay of stiffness with the strain level, by comparison with the stiffness decay curves of the elements on the centerline back-figured from the observed embankment behavior under increasing loading. **DOI: 10.1061/(ASCE)GT.1943-5606.0000965.**

Author keywords: Dilatometers; Cone penetration tests; Stress history; Stiffness; Sand; Silts.

Introduction

In the past decades, comprehensive geotechnical investigations have been carried out to characterize Venice soils in relation to the design and construction of various engineered solutions aimed at reducing the frequency of flooding, including huge movable gates located at the three lagoon inlets. The Venice lagoon soil deposits are highly heterogeneous and characterized by a predominant silt fraction, combined with sand and/or clay, forming a chaotic interbedding of various sediments. The basic mineralogical components of the lagoon sediments do not vary appreciably as a result of similar geological origin and common depositional environment. These low-plasticity silty soils are extremely sensitive to stress relief and disturbance as a result of sampling (Cola and Simonini 1999, 2002). The difficulty in obtaining soil properties in the laboratory pushed toward the use of in situ testing; in particular, seismic dilatometer (SDMT) tests and piezocone (CPTU) tests, in combination with a full-scale trial embankment constructed at the Treporti test site (TTS). This paper focuses mainly on the evaluation of overconsolidation and stiffness of the TTS soils from the combined use of SDMT and CPTU test results, based on the observed embankment response.

Treporti Test Site: Embankment, Site Investigations, and Soil Description

At the TTS a sand trial embankment was constructed between September 2002 and March 2003. The bank (Fig. 1) had a 40-m-diameter cylindrical form, which was realized with 13 superposed 0.5-m-thick layers sustained by a 6.7-m-high geogrid-reinforced vertical wall and applied a uniform pressure of 106 kPa to the ground surface. The bank was continuously monitored for pore-water pressures, surface settlements, and horizontal and vertical displacements with depth (for details, see Simonini 2004). The monitoring continued for almost 4 years after construction as well as throughout the gradual removal of the embankment (from June 2007 to March 2008). A crucial role in monitoring the field response under the trial bank was played by sliding deformeters (SDs) (Kovari and Amstad 1982), which provided accurate measurements of local vertical strains in the soil at 1-m-deep intervals in four different locations under the bank. Fig. 2 shows the construction time history of the bank and the associated surface settlement measured at the center.

The bank area was extensively investigated by CPTU tests (Gottardi and Tonni 2004; Tonni et al. 2010; Tonni and Gottardi 2011),

[1]Assistant Professor, Dept. of Civil, Architectural and Environmental Engineering, Univ. of L'Aquila, Via Giovanni Gronchi 18, 67100 L'Aquila, Italy (corresponding author). E-mail: paola.monaco@univaq.it

[2]Visiting Research Fellow, Dept. of Civil, Architectural and Environmental Engineering, Univ. of L'Aquila, Via Giovanni Gronchi 18, 67100 L'Aquila, Italy. E-mail: sara.amoroso@gmail.com

[3]Professor, Dept. of Civil, Architectural and Environmental Engineering, Univ. of L'Aquila, Via Giovanni Gronchi 18, 67100 L'Aquila, Italy. E-mail: silvano@marchetti-dmt.it

[4]Engineer, Studio Prof. Marchetti, Via Bracciano 38, 00189 Roma, Italy. E-mail: diego@marchetti-dmt.it

[5]Associate Professor, Dept. of Civil, Architectural and Environmental Engineering, Univ. of L'Aquila, Via Giovanni Gronchi 18, 67100 L'Aquila, Italy. E-mail: gianfranco.totani@univaq.it

[6]Associate Professor, Dept. of Civil, Architectural and Environmental Engineering, Univ. of Padova, Via Ognissanti 39, 35129 Padova, Italy. E-mail: simonetta.cola@unipd.it

[7]Professor, Dept. of Civil, Architectural and Environmental Engineering, Univ. of Padova, Via Ognissanti 39, 35129 Padova, Italy. E-mail: paolo.simonini@unipd.it

Note. This manuscript was submitted on June 27, 2012; approved on May 10, 2013; published online on May 14, 2013. Discussion period open until June 1, 2014; separate discussions must be submitted for individual papers. This paper is part of the ***Journal of Geotechnical and Geoenvironmental Engineering***, Vol. 140, No. 1, January 1, 2014. ©ASCE, ISSN 1090-0241/2014/1-215–227/$25.00.

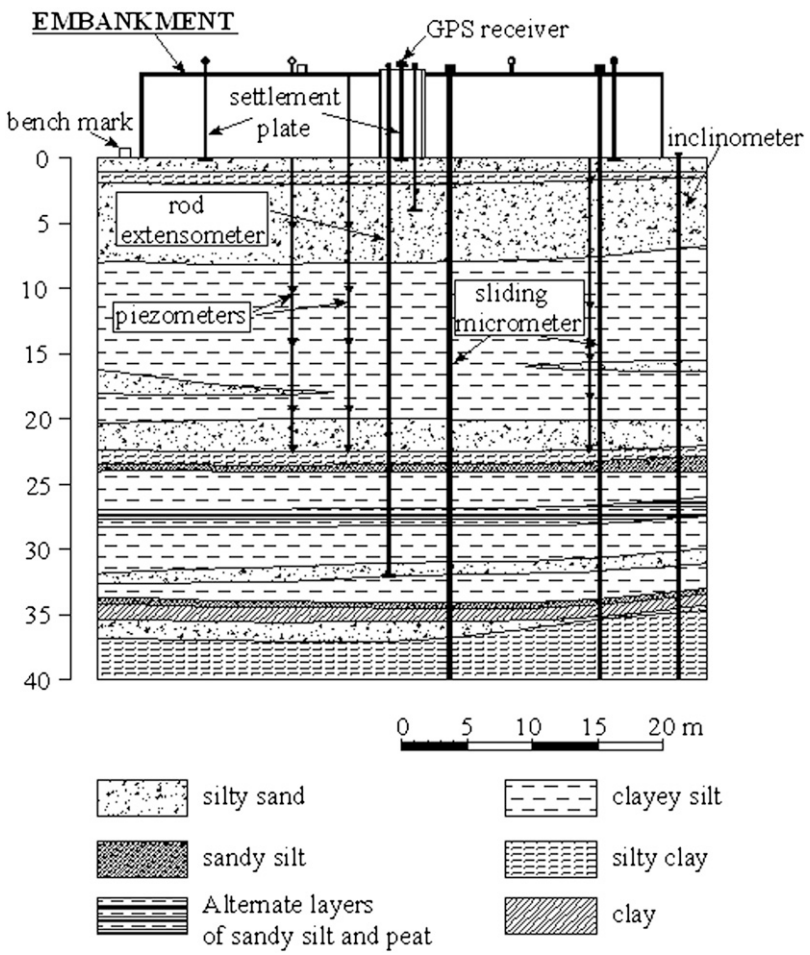

Fig. 1. Cross section of the embankment with soil profile and monitoring devices (data from Simonini et al. 2007)

flat dilatometer (DMT) tests (Marchetti et al. 2004, 2006), seismic CPTU and DMT tests (SCPTU-SDMT) (McGillivray and Mayne 2004), and continuous coring boreholes and high-quality laboratory tests (Simonini 2004; Simonini et al. 2007). The DMT-SDMT and CPTU-SCPTU soundings were executed in the following three different phases (Fig. 2):

- Site Investigation 1 (SI-1): before starting the construction of the embankment (in 2002);
- Site Investigation 2 (SI-2): at the end of construction, from the top of the embankment (in 2003); and
- Site Investigation 3 (SI-3): after completing the gradual removal of the embankment (in 2008).

Fig. 3 summarizes the soil profile at the TTS and the basic soil properties determined from the laboratory samples. The upper portion of the deposit consists of a medium-fine silty sand layer (2–8 m in depth), located below a thin soft silty clay layer and followed by a clayey-sandy silt layer (8–20 m). Below 20 m of depth, the soil is mostly composed of alternating layers of clayey and sandy silt. Frequent laminations of peat are encountered below 25 m. Fig. 3 also shows the CPTU test results (corrected cone resistance q_t, sleeve friction f_s, and pore pressure u_2) obtained at the center of the embankment in SI-1 (before construction).

Ten DMT and CPTU soundings were executed at nearby locations before construction. At the end of construction and after removal of the embankment DMT and CPTU were executed at three locations (14, 19, and 20 in Fig. 2). SDMTs, a combination of the mechanical DMT with an add-on seismic module for measuring the shear wave velocity V_S (for details, see Marchetti et al. 2008), were performed at three locations before construction, in conjunction with SCPTU tests (McGillivray and Mayne 2004), and after removal of the embankment.

Fig. 4 shows the profiles of the DMT parameters (namely, material index I_D, constrained modulus M, undrained shear strength c_u, and horizontal stress index K_D) obtained using common correlations (Marchetti 1980; Marchetti et al. 2001) from DMT 14 at the center of the embankment as well as the profiles of V_S obtained from SDMT 14, 15, and 19 (McGillivray and Mayne 2004), in SI-1. Fig. 5 shows the side-by-side profiles of K_D obtained in SI-1 from DMT 11, 15, 14, and 19, along a diameter section of the embankment. Fig. 5 clearly shows the intermittent character of the stiff sand layer at about 16–17 m. Fig. 6 compares the profiles obtained from DMT-SDMT 19 as well as the corresponding profiles of q_t obtained from CPTU 19 in the three investigation phases, SI-1, SI-2, and SI-3. The results of the investigations have been used in two different ways; i.e., (1) to predict the embankment behavior and compare it with the observed behavior, and (2) to observe changes in the supporting soil following embankment loading/unloading.

J. Geotech. Geoenviron. Eng. 2014.140:215-227.

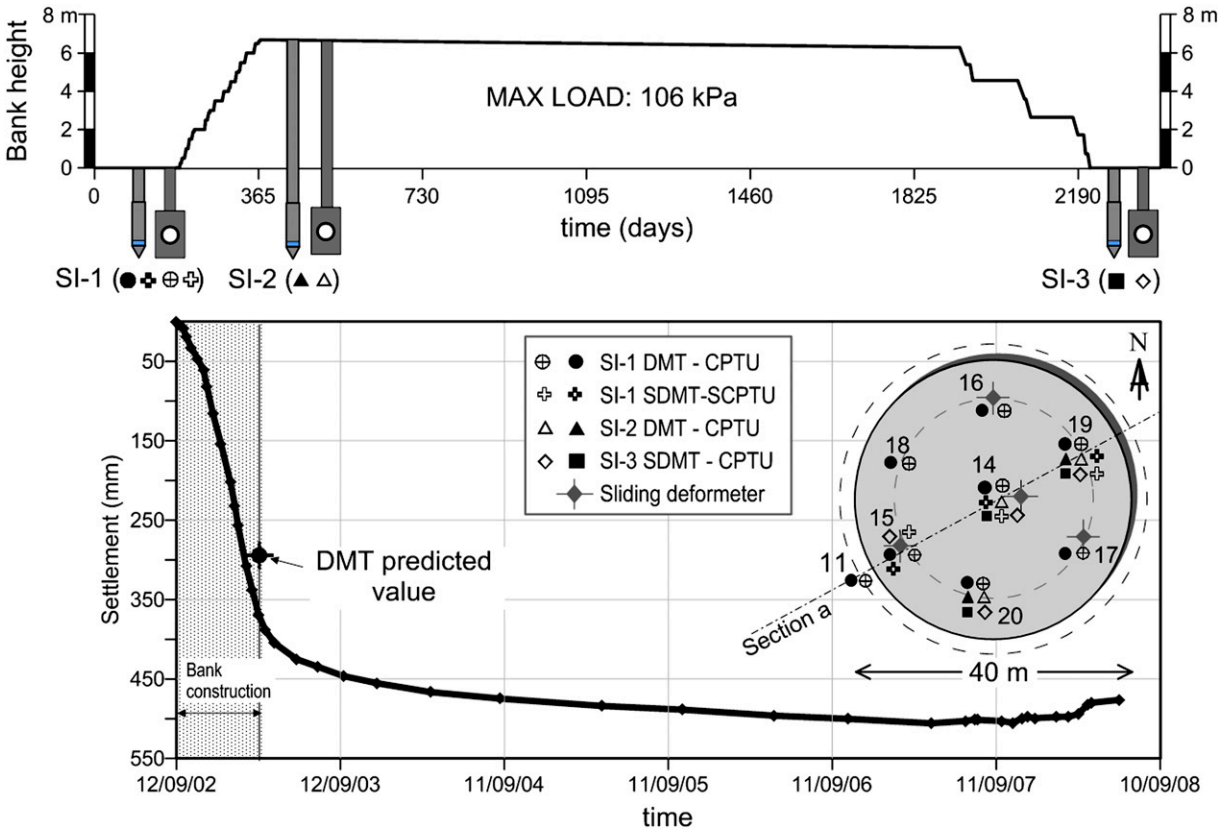

Fig. 2. Loading program, settlement-time evolution at the bank center, and schematic location of DMT-CPTU investigations and SDs

Displacements and Compression Curves from Field Measurements

Fig. 7 depicts the evolution of settlements of the ground surface at the half-bank, on completion, after 4 years at constant load and after bank removal. The central settlement after 4 years was 50.5 cm, 12.4 cm of which (a high 25%) secondary compression occurred at constant load after bank completion. The piezometer readings indicated no excess pore pressure in any layer under increasing load, suggesting that the primary consolidation was quite rapid and contemporary with the bank construction.

Fig. 8(a) shows the load-settlement curve, where it can be recognized that there is an initial branch in which the slope is modest, and then a nearly linear branch considerably steeper. It is plausible that in the initial branch the stresses in most elements had not exceeded the preconsolidation stress. In the subsequent branch the near linearity is a result of various opposite-sign phenomena; i.e., the moduli increase as the consolidation progresses but decrease with increasing shear strain and also decrease when stresses overcome the preconsolidation stress. Each element below the center of the embankment follows a different stress path [Fig. 8(b)], whose slope in the s'-t plane (or, alternatively, in the p'-q plane) increases with depth. Thus, the settlement at the surface is the summation of contributions of elements experiencing the previously listed phenomena in various proportions and at various times.

The maximum horizontal displacements observed by the inclinometers below the perimeter (≈50 mm) were one order of magnitude lower than the maximum vertical settlements throughout the whole construction period; i.e., the deformation process developed prevalently in the vertical direction (Simonini et al. 2007). During unloading the soil exhibited a very stiff response characterized by a small settlement recovery (≤30 mm), as the last part of the graph in Fig. 2 indicates.

The SDs provided measurements of local vertical strains of 1-m-thick layers throughout the complete loading-unloading sequence. The distribution of vertical strains with depth is shown in Fig. 9(a) and in an accumulated form in Fig. 9(b). The prevalent contributions of the thin silty clay layer at ≈1–2 m in depth and of the silt layer between 8 and 20 m are evident. The strains decreased with depth, and below 35 m were not detectable by the instruments. After bank removal the observed settlement recovery was very small (≈6% of the total vertical settlement at the center), as highlighted by the dashed area in Fig. 9(b).

Fig. 10 shows typical field compression curves (1-m field oedometers) in sands and silts under the bank center. The vertical strains ε_v were measured by a SD in each 1-m-thick layer. The vertical stress increments were estimated using the theory of elasticity solution for a circular uniform surface load. Each diagram starts from the geostatic vertical effective stress σ'_{v0}. In Fig. 10 a much stiffer response at the beginning of the loading phase and a much softer response beyond a threshold stress (more recognizable in silt than in sand) is seen. At the end of the loading phase the deformation process is characterized by significant creep, followed by a very stiff unloading response with small settlement recovery. Because strains in the ground developed prevalently in the vertical direction, it was tentatively assumed that the curves in Fig. 10 may be viewed as a sort of 1-m field oedometer curve and that the threshold stress may be considered as preconsolidation stress. However, as discussed previously, the 1-m field oedometers are, strictly speaking, not oedometers because the various stress paths upon loading are below/above the K_0 line.

J. Geotech. Geoenviron. Eng. 2014.140:215-227.

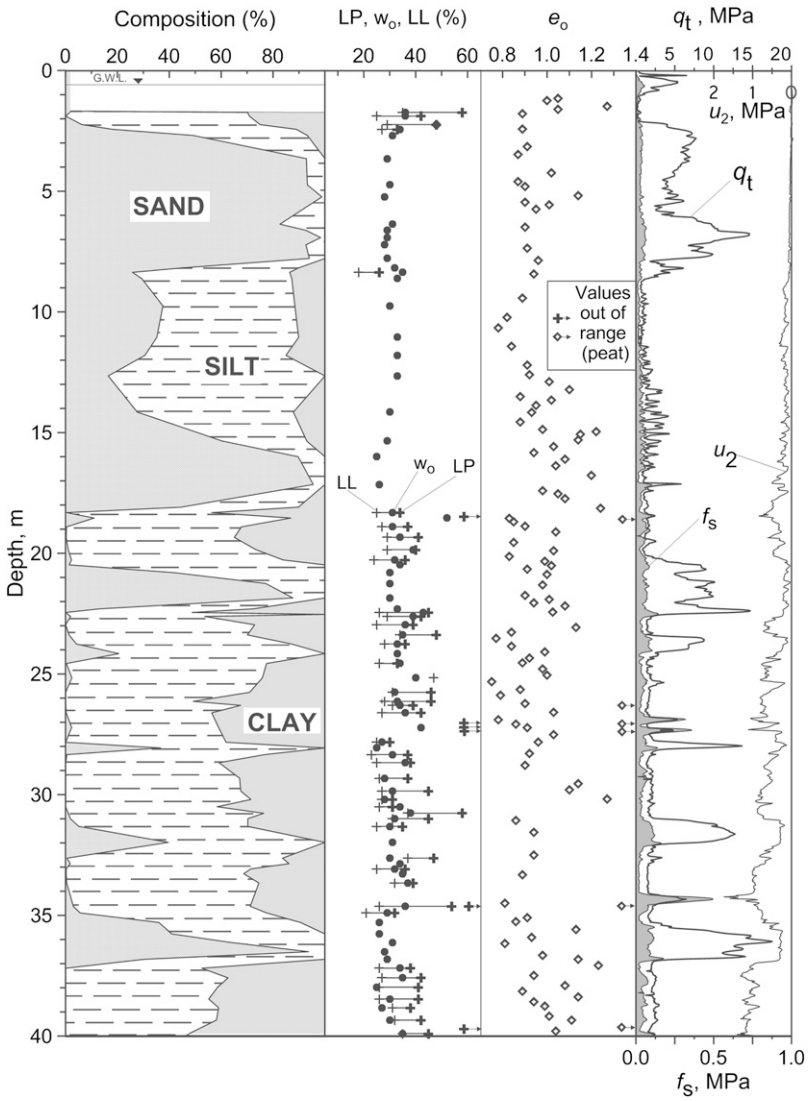

Fig. 3. Soil composition, basic properties, and CPTU profiles at the TTS (data from Simonini et al. 2007)

Evaluation of Overconsolidation Ratio in Sand from Dilatometer and Piezocone Tests

Reference Overconsolidation Ratio Profiles for Constructing the Correlations

The OCR profiles under the center of the embankment were known (based directly on the OCR definition $\mathrm{OCR} = \sigma'_{v\,\max}/\sigma'_{v0}$) at two times; i.e., at full load (Fig. 11, profile *b*) and after load removal (Fig. 11, profile *c*). At full load it was considered to be $\mathrm{OCR} \approx 1$, assuming (based on Fig. 10) that at every depth the vertical stress had exceeded the maximum past pressure (however, this condition may not have occurred locally in certain stiffer inclusions outside the bank centerline, as explained subsequently). After load removal the OCR was evaluated assuming $\sigma'_{v\,\max}$ as the geostatic stress plus the vertical stress increment induced by the uniformly loaded circular area, according to the theory of elasticity. Fig. 11 also includes a tentative OCR profile (Fig. 11, profile *a*) of the undisturbed soil before loading, based on the maximum curvature points in Fig. 10. The latter profile suggests, in the upper $\approx$8 m, light overconsolidation, possibly as a result of erosion that occurred during the Pleistocene, combined with the effects of waves/tides, aging, and desiccation.

Format of the Overconsolidation Ratio Correlations

Correlations OCR-DMT in sand have been attempted by Schmertmann (1983), Marchetti (1985), and Mayne et al. (2009). Correlations K_D-OCR have also been established for some sites but with local applicability. The method currently considered more generally applicable, although highly approximate, is the method described in Marchetti et al. (2001) that makes use of the ratio between the constrained modulus M from DMT (M_{DMT}) and the cone penetration resistance q_c from the cone penetration test (CPT). The semiquantitative guidelines reported in Marchetti et al. (2001) are $M_{\mathrm{DMT}}/q_c = 5-10$ in normally consolidated (NC) sands and $M_{\mathrm{DMT}}/q_c = 12-24$ in overconsolidated (OC) sands.

The root of the method is the following. As is widely known, the α factor by which the tip resistance q_c has to be factorized, to get an estimate of the operative Young's modulus E', increases significantly with the OCR. Extensive calibration chamber research on sands (e.g., Baldi et al. 1989) has indicated typical α values $\approx$3–4 in NC sand and up to $\approx$20 in OC sands. Because the ratio α increases with the OCR, it may be used as an indicator of the OCR. Similarly, although in the opposite direction, Devincenzi and Canicio (2001) found that saturating a loess caused a destructuration, a sort of OCR reduction, reflected by a drop of $\alpha = M_{\mathrm{DMT}}/q_c$ from 20 to 8.

J. Geotech. Geoenviron. Eng. 2014.140:215-227.

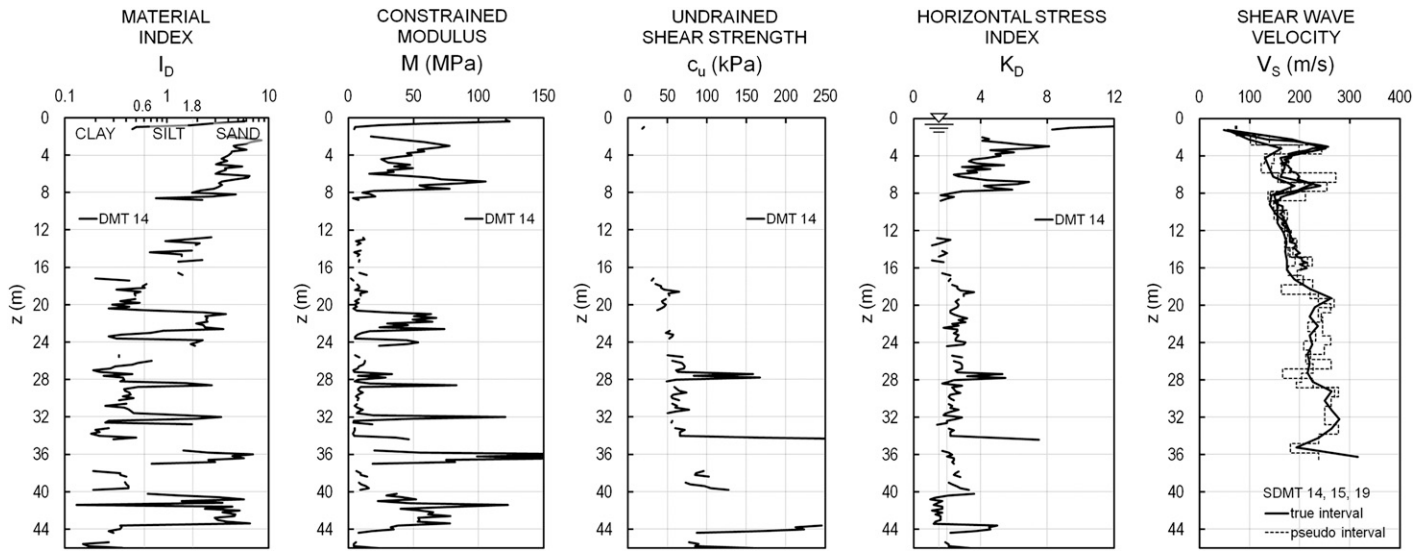

Fig. 4. Profiles of soil parameters from DMT 14 at the bank center (Marchetti et al. 2004) and V_S profiles from SDMT 14, 15, and 19 (McGillivray and Mayne 2004) before embankment construction

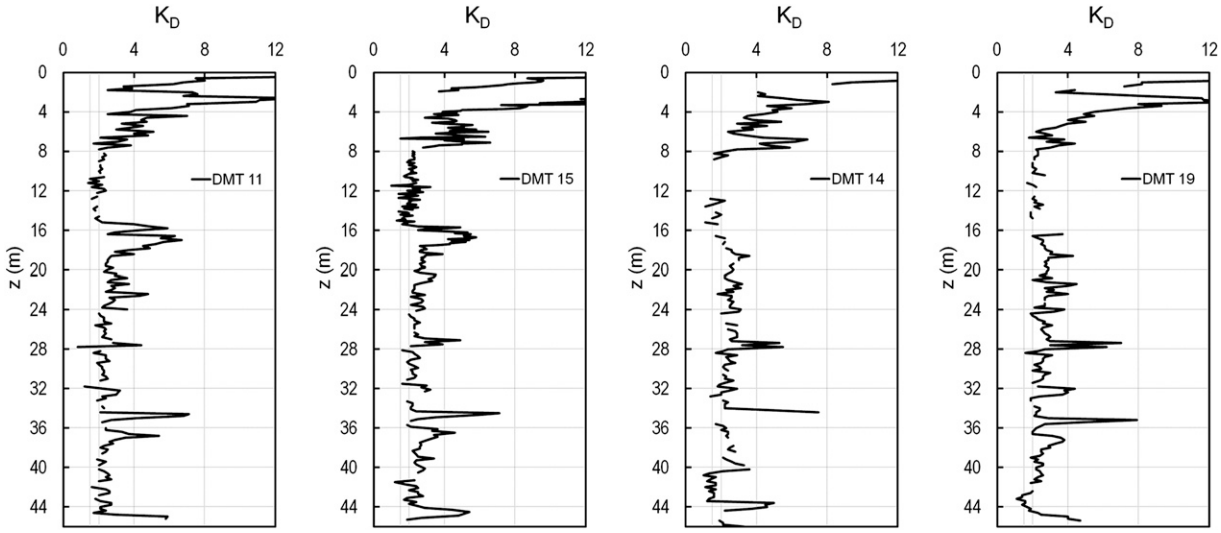

Fig. 5. Profiles of the horizontal stress index K_D along a diameter section of the embankment (Section a in Fig. 2) before construction

Additional support for the increase of α with the OCR derives from several studies demonstrating the higher sensitivity of M_{DMT} compared with q_c in monitoring densification; for instance, Jendeby (1992) measured q_c and M_{DMT} before and after the compaction—and stress history increase—of a loose sand fill and found that the compaction increased both; however, M_{DMT} increased more significantly (α before compaction = 7–9; α after compaction = 12–22). In summary, because moduli increase with the OCR at a faster rate than the penetration resistance, the ratio between the modulus and penetration resistance should increase with the OCR.

Correlations Overconsolidation Ratio-M_{DMT}/q_t and Overconsolidation Ratio-K_D in Sand

Fig. 12(a) shows the correlation OCR-M_{DMT}/q_t for the TTS sands. It was constructed using the same depth values of M_{DMT} and q_t obtained from Soundings 14, 19, and 20 in sand layers (with material index $I_D > 1.8$) between 2- and 35-m depth. The DMT/CPTU data were those obtained at the times when the reference OCR profiles were available (Fig. 11, profiles *b* and *c*); i.e., at end of construction and postremoval. The preconstruction OCRs back-figured from the 1-m field oedometer (Fig. 11, profile *a*) were intentionally not used to derive the correlation OCR-M_{DMT}/q_t in Fig. 12(a), assuming such an OCR was less reliable than the imparted OCR because they could be affected by some uncertainty in the interpretation (particularly in sand, which often lacks a well-defined breakpoint in the in situ compression curves). The data pairs M_{DMT}/q_t from SI-2 and SI-3, reported in Table 1, were carefully selected to avoid any possible mismatching of data by retaining only pairs from uniform soil layer of significant thickness. The equation of the interpolating line is

$$\text{OCR} = 0.0344(M_{DMT}/q_t)^2 - 0.4174(M_{DMT}/q_t) + 2.2914 \quad (1)$$

The OCR-M_{DMT}/q_t data points in Fig. 12(a) are either in good agreement with the TC16 guidelines (Marchetti et al. 2001)

J. Geotech. Geoenviron. Eng. 2014.140:215-227.

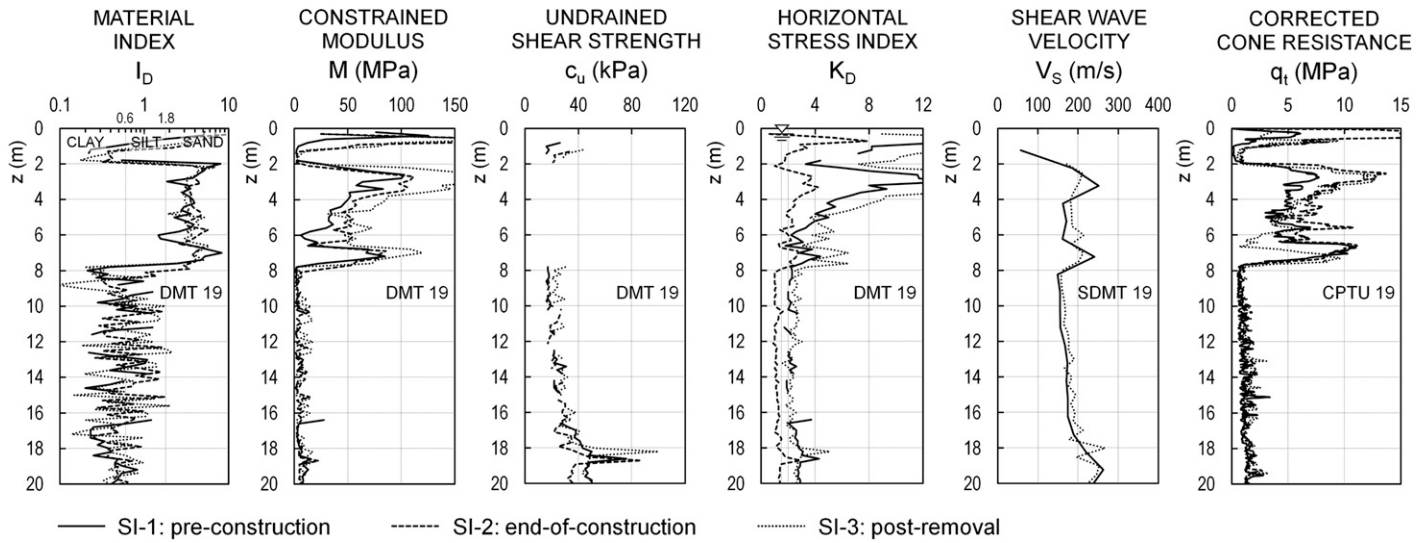

Fig. 6. Profiles of the soil parameters from DMT-SDMT 19 and the corrected cone resistance q_t from CPTU 19 before construction, at the end of construction, and after removal of the embankment

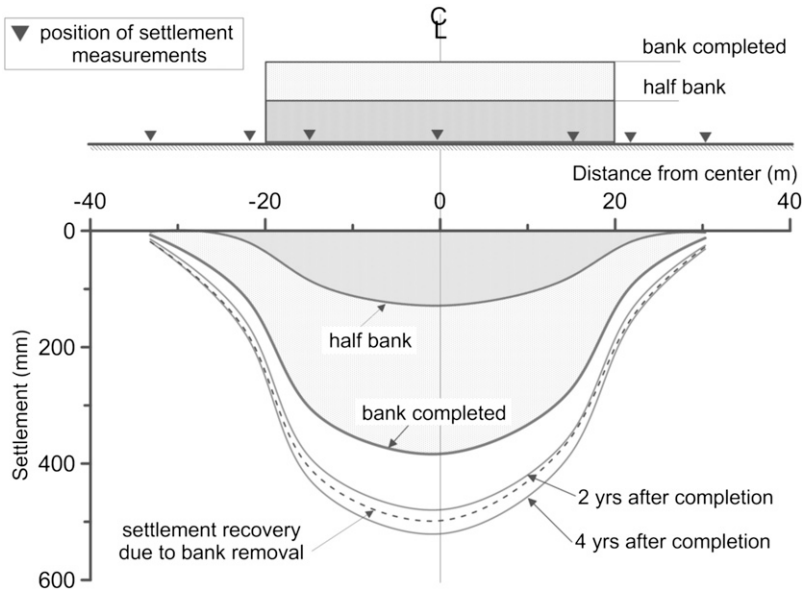

Fig. 7. Settlements of the ground surface along a diameter section at various times of the bank life

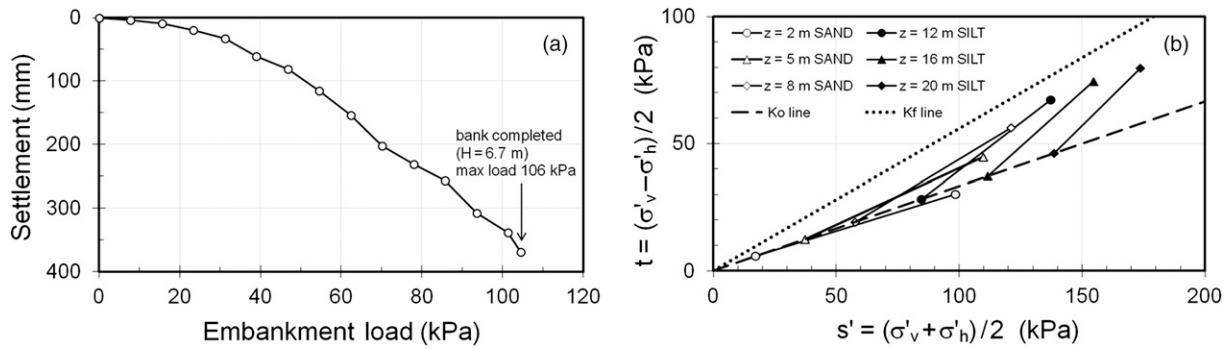

Fig. 8. (a) Load-settlement curve and (b) stress paths at various depths under the embankment center during construction (with $\Delta\sigma'_v$ and $\Delta\sigma'_h$ calculated by the elasticity solution theory for a circular uniform surface load on a semiinfinite homogeneous soil space)

J. Geotech. Geoenviron. Eng. 2014.140:215-227.

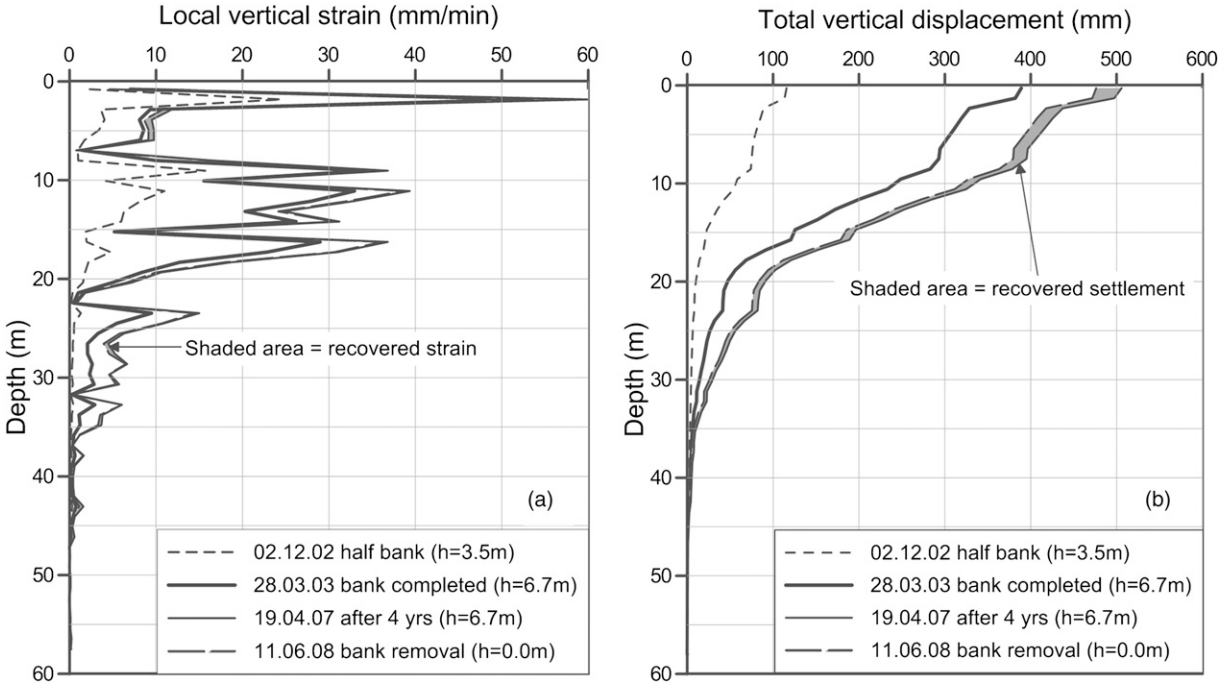

Fig. 9. (a) Local vertical strain and (b) total vertical displacement measured by a SD close to the bank center

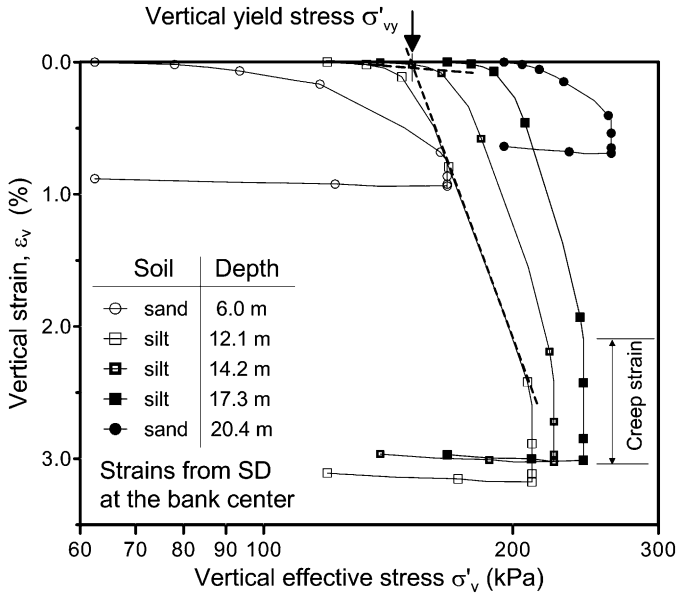

Fig. 10. Typical field compression curves (1-m field oedometer) in sands and silts (data from Simonini et al. 2007)

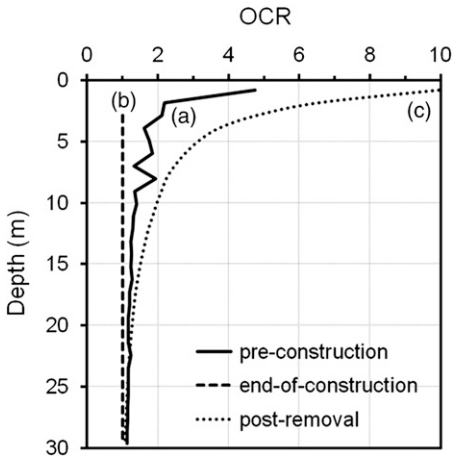

Fig. 11. OCR profiles: (a) before construction; (b) at the end of construction; (c) after removal of the embankment (at the center)

($M_{DMT}/q_c = 5-10$ in NC sands; $M_{DMT}/q_c = 12-24$ in OC sands) and the previously mentioned existing experimental base relative to other sands. These trends appear to support each other and may possibly provide broad OCR estimates in a number of sand sites in the Venetian area and the closest mainland.

As indicated by previous calibration chamber research (Jamiolkowski et al. 1988), the OCR-M_{DMT}/q_t relationship is also dependent, at least moderately, on the relative density D_r and the stress level, and is possibly influenced by sand type and cementation. The experimental data obtained at the TTS, mostly in medium dense ($D_r \approx 50-80\%$) sands and in a limited range of vertical stress, do not permit definitely assessing the dependency of the OCR-M_{DMT}/q_t relationship on the previous parameters. However, a relationship based on full-scale testing in situ should represent real-life experimental evidence not subjected to possible calibration chamber artifacts.

Fig. 12(b) shows the correlation OCR versus K_D in sand, constructed in a similar way. The dispersion of the correlations OCR-M_{DMT}/q_t and OCR-K_D in Figs. 12(a and b) is very similar; i.e., the regression coefficient shows good values in both cases ($r^2 = 0.927-0.917$), indicating that the OCR has an important influence on both dimensionless quantities. However, previous studies (Marchetti 1985; Schmertmann 1983) have indicated that in sands the correlation between the coefficient of earth pressure at rest K_0 (hence, the OCR) and K_D depends also on relative density

J. Geotech. Geoenviron. Eng. 2014.140:215-227.

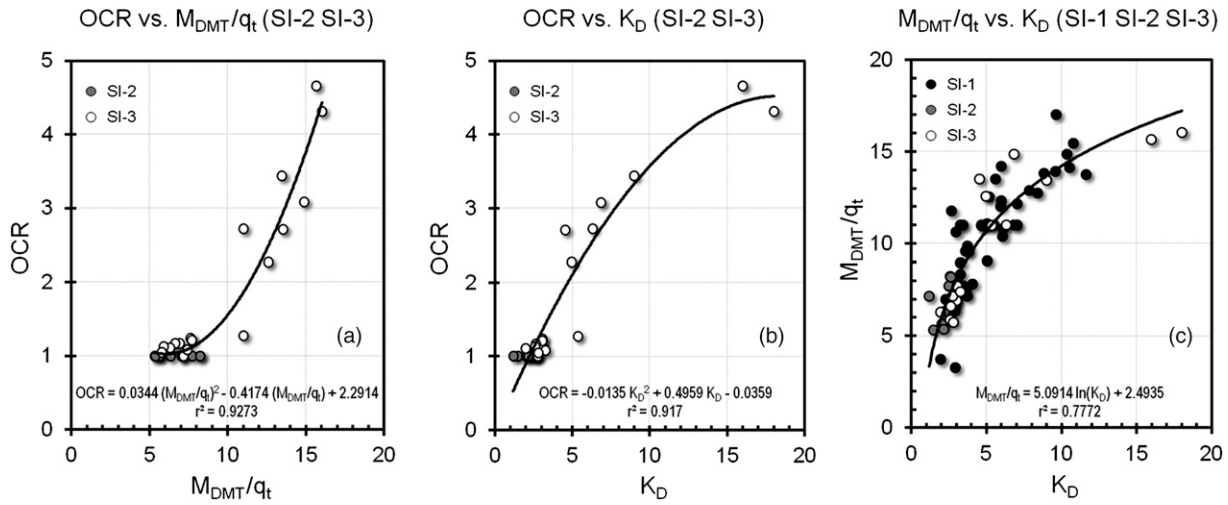

Fig. 12. (a) Correlation OCR-M_{DMT}/q_t and (b) correlation OCR-K_D constructed using DMT and CPTU data (soundings 14, 19, and 20) from end-of-construction (SI-2) and postremoval (SI-3) site investigations; (c) correlation M_{DMT}/q_t-K_D constructed using DMT and CPTU data from all site investigations (SI-1, SI-2, and SI-3) (all data points refer to sand layers having material index $I_D > 1.8$ between 2- and 35-m depth)

Table 1. End-of-Construction and Postremoval DMT-CPTU and OCR Data Used to Derive the Correlation OCR-M_{DMT}/q_t [Eq. (1)]

Site investigation	Sounding number	Depth (m)	σ'_v (kPa)	I_D (−)	K_D (−)	M_{DMT} (MPa)	q_t (MPa)	M_{DMT}/q_t (−)	OCR (−)
SI-2	19	3.20	161	3.96	2.59	80.4	9.8	8.2	1.00
SI-2	19	4.30	178	3.64	2.51	55.9	7.2	7.7	1.00
SI-2	19	7.10	224	3.96	2.63	80.8	9.8	8.2	1.00
SI-2	19	22.10	466	2.45	2.59	41.5	5.9	7.0	1.00
SI-2	19	24.20	502	2.30	2.08	44.7	7.9	5.7	1.00
SI-2	20	3.00	158	5.81	2.19	67.8	10.7	6.3	1.00
SI-2	20	6.70	216	5.11	1.49	40.9	7.7	5.3	1.00
SI-2	20	17.50	387	2.97	2.03	58.0	10.3	5.6	1.00
SI-2	20	23.60	492	1.90	1.18	39.9	5.6	7.2	1.00
SI-2	20	32.20	644	1.90	2.16	54.3	10.1	5.4	1.00
SI-3	14	21.50	409	1.93	3.05	55.1	7.2	7.6	1.24
SI-3	14	23.60	448	1.90	3.02	54.5	7.9	6.9	1.17
SI-3	14	31.60	600	1.90	2.76	68.1	9.5	7.2	1.00
SI-3	19	2.80	53	3.55	15.97	162.8	10.4	15.7	4.66
SI-3	19	4.00	76	2.97	9.00	85.1	6.3	13.4	3.44
SI-3	19	4.60	87	3.27	6.84	71.8	4.8	14.9	3.08
SI-3	19	5.40	103	4.30	4.54	57.2	4.2	13.5	2.71
SI-3	19	7.00	133	4.22	4.95	97.9	7.8	12.6	2.27
SI-3	19	21.50	409	1.90	3.03	51.2	6.6	7.7	1.21
SI-3	19	23.60	448	2.02	2.63	43.5	6.6	6.6	1.17
SI-3	19	28.10	534	2.53	1.96	34.3	5.5	6.3	1.11
SI-3	19	31.50	599	1.96	3.24	74.5	10.1	7.4	1.08
SI-3	20	3.00	57	2.97	18.00	156.9	9.8	16.0	4.31
SI-3	20	5.40	103	3.12	6.32	69.1	6.3	11.0	2.72
SI-3	20	17.70	336	2.21	5.35	117.7	10.7	11.0	1.27
SI-3	20	24.10	458	2.27	2.59	44.5	7.6	5.9	1.13
SI-3	20	32.50	618	1.80	2.79	60.9	10.6	5.7	1.05

Note: End-of-construction data for site investigation SI-2, OCR = profile *b* in Fig. 11; postremoval data for site investigation SI-3, OCR = profile *c* in Fig. 11.

D_r or friction angle φ'. Therefore, the OCR-K_D correlation in Fig. 12(b) probably only has local validity for the Treporti sand.

In this study it was also found appropriate to check if M_{DMT}/q_t and K_D are themselves correlated, considering the intended use of both in predicting the OCR. Fig. 12(c) shows several M_{DMT}/q_t-K_D data pairs obtained in sand layers ($I_D > 1.8$) between 2- and 35-m depth from all DMT soundings carried out in all site investigation phases (SI-1, SI-2, and SI-3). The trend in Fig. 12(c) suggests that M_{DMT}/q_t and K_D are basically interrelated and largely involve similar information; hence, the possible combined use of both for estimating the OCR would not add any substantial benefit.

The diagram shown in Fig. 13 was subsequently constructed to compare the preconstruction OCR predicted by Eq. (1), using M_{DMT}/q_t data pairs from all DMT and CPTU soundings carried out

in SI-1 (in the centrum but also close to the external circumference), with the OCR of the original soil back-figured from the 1-m field oedometer (Fig. 11, profile *a*). The preconstruction OCR and M_{DMT}/q_t were not included in the data set used to obtain Eq. (1), which was calibrated based only on the end-of-construction and postremoval OCRs (Fig. 11, profiles *b* and *c*) associated with M_{DMT}/q_t from SI-2 and SI-3 (see Table 1).

The comparison in Fig. 13 shows that the OCRs estimated by Eq. (1) are generally higher than the OCR back-figured from the 1-m field oedometer. In particular, at depths of ≈16−17 m some data points obtained by Eq. (1) exhibit OCRs between 1.8 and 2.4, well beyond the back-figured original OCR ≈ 1.2, and even beyond the dashed line initially assumed as a known OCR profile for calibration. At first glance, these high OCR values predicted by Eq. (1) appear to be excessive. However, at the same test depths the corresponding DMT and CPTU profiles, in particular the K_D profiles (see, e.g., DMT 11 and 15 in Fig. 5), clearly indicate the presence of a stiffer sand layer, which on the other hand is not found at the center of the embankment (DMT 14) where the OCRs from the 1-m field oedometer were back-figured. Therefore, the OCR ≈ 1.8−2.4 predicted by Eq. (1) at about 16- to 17-m depth, at certain test locations, appear to reflect the presence of a higher OC sand layer, not continuously crossing the embankment area, where the vertical stress at full load may not have exceeded the maximum past pressure. In other words, the dashed lines in Figs. 11 and 13, initially assumed to be the known OCR profiles for calibration, appear to have underestimated the initial OCR in layers such as those at 16–17 m in DMT 11 and 15 in Fig. 5.

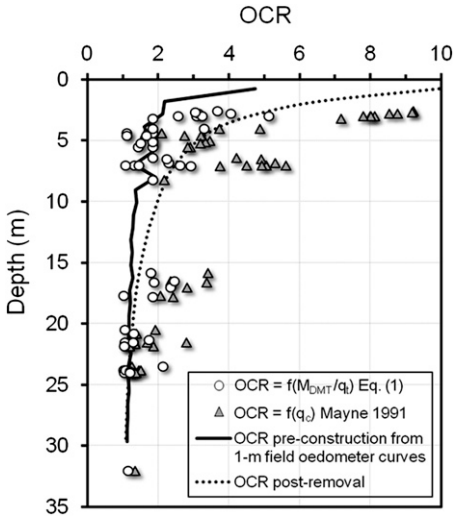

Fig. 13. Comparison of OCR profiles of the original soil back-figured from 1-m field oedometer curves (profile *a* in Fig. 11), OCR estimated by M_{DMT}/q_t [Eq. (1)] and OCR estimated by q_t only (Mayne 1991) using data obtained in sand from all preconstruction DMT and CPTU soundings

As an additional verification, the OCR values predicted by Eq. (1) were compared with the OCR predicted by the CPT-based correlation proposed by Mayne (1991), using q_t from SI-1 (although it is recognized that determining the stress history in sands by methods based on the penetration resistance involves a serious uncertainty). This comparison, also shown in Fig. 13, indicates that the OCRs estimated from q_t at ≈16- to 24-m depth are similar to the high OCRs predicted by Eq. (1) at the same test locations. However, the OCRs predicted according to Mayne (1991) show, in general, a higher scatter and tend to overestimate the OCR of the original soil back-figured from the 1-m field oedometer, especially at shallow depths.

Increase of V_S, M_{DMT}, K_D, and q_t Caused by Overconsolidation

The comparisons in Fig. 14 illustrate how the SDMT, DMT, and CPTU results reacted to the overconsolidation caused by the embankment. Attention is concentrated here on the sand layer between 2 and 8 m depth. Fig. 14 compares the original (preconstruction) profiles of V_S, M_{DMT}, K_D, and q_t with the postremoval profiles; because all the profiles refer to green grass (i.e., without embankment), the only difference is the leftover overconsolidation caused by the embankment. It appears that the overconsolidation effect is reflected almost negligibly by V_S (or by the small strain shear modulus G_0 derived from V_S), to a maximum degree by M_{DMT}, which doubles in value with the OCR, to a medium degree by q_t. The increase of M_{DMT} (interpreted from the dilatometer modulus E_D and from K_D) is essentially a result of the increase of K_D. Incidentally, the q_t measured postremoval below 6 m in Fig. 14 shows an unexpected decrease—rather than an increase—with the OCR. As also noted by Tonni and Gottardi (2011), this inconsistency is probably related to the high horizontal spatial variability of the subsoil.

It is worth noting the parallelism between the in situ trend observed at the TTS and the trend observed in previous laboratory researches. For instance, Yamashita et al. (2000) showed that the benefit of the OCR on the modulus is practically negligible at small strains, maximum at operative strains, and modest at high strains. These results suggest that the DMT, in particular K_D, is considerably more sensitive than q_t to the stress history. This finding is in line with previous experimental data; see, for instance, the Marchetti (2010) compilation of cases in the literature showing the higher reactivity

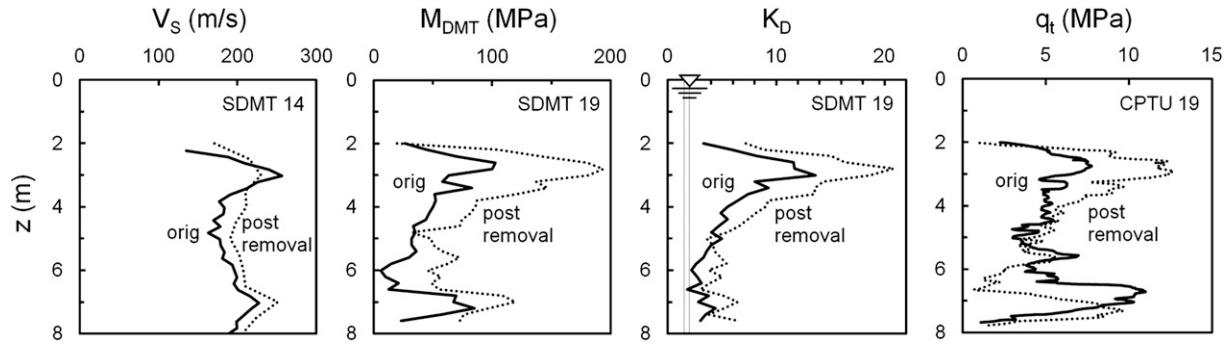

Fig. 14. Influence on the various parameters of the overconsolidation caused by the TTS embankment (sand layer between 2- and 8-m depth)

J. Geotech. Geoenviron. Eng. 2014.140:215-227.

of K_D to stress history or the recent extensive series of comparative CPT and DMT in the calibration chamber by Lee et al. (2011), who found that overconsolidation (OCR = 2−8) increased the normalized q_c by a factor of 1.10–1.15 and K_D by a factor of 1.30–2.50.

Stiffness from Dilatometer and Seismic Dilatometer Tests versus Observed Embankment Response

Dilatometer Test Predicted versus Observed Settlements and Moduli

The settlements at the TTS were predicted by the DMT (Marchetti et al. 2004) using the simple one-dimensional (1D) classic Terzaghi approach $S = \sum(\Delta\sigma_v/M_{DMT})\Delta z$, with the vertical stress increments $\Delta\sigma_v$ calculated by the theory of elasticity solution for a circular uniform surface load, extending the calculation down to a depth at which $\Delta\sigma_v/\sigma'_{v0} = 0.10$ (i.e., ≈38−39 m at the center). The settlement predicted by M_{DMT} (which does not include secondary compression) using the 1D approach was 29 cm, in reasonable agreement with the total surface settlement of ≈38 cm measured under the center of the embankment at the end of construction (180 days, see Fig. 2), which includes some secondary compression during construction.

As previously introduced, a 1D deformation condition may be tentatively hypothesized under the bank centerline. In this hypothesis, the in situ constrained modulus M may be calculated as $M = \Delta\sigma_v/\varepsilon_v$, where ε_v are the local vertical strains measured by a SD under the bank center at the end of construction, and $\Delta\sigma_v$ are evaluated at the midheight of each 1-m soil layer by linear elasticity formulas. The profile of the back-calculated in situ constrained modulus M [Fig. 15(a)] is in overall satisfactory agreement with the profile of M_{DMT}. A similar agreement was observed between the profiles of ε_v measured by a SD under the bank center at the end of construction and that calculated by M_{DMT} as $\varepsilon_v = \Delta\sigma_v/M_{DMT}$ [Fig. 15(b)], as well as between the corresponding profiles of observed and DMT-predicted settlement S at each depth [Fig. 15(c)]. The previous comparisons support the assumption that M_{DMT} is a reasonable estimate of the constrained operative or working strain modulus (i.e., the modulus that, when introduced into the linear elasticity formulas, provides realistic estimates of the settlement of a shallow foundation under working loads), as suggested by a large number of documented comparisons between measured and DMT-predicted settlements (Monaco et al. 2006).

In Situ Decay Curves of Stiffness with Strain Level

Besides the moduli at the end of construction, moduli were also back-calculated in the elements on the centerline from local vertical strains ε_v measured during construction under each load increment (from small to working strains). The stiffness considered in this section is the Young's modulus E.

In situ secant Young's moduli E were back-calculated at the midheight of each 1-m soil layer as $E = (\Delta\sigma_v - 2\nu\Delta\sigma_r)/\varepsilon_v$, assuming vertical and radial stress increments $\Delta\sigma_v$ and $\Delta\sigma_r$ according to the theory of elasticity, from local ε_v measured by a SD at the center of the embankment under each load increment during construction (Marchetti et al. 2006). Fig. 16(a) shows the moduli corresponding to the first construction step ($H = 0.5$ m), half-bank ($H = 3.5$ m), and construction end ($H = 6.7$ m). For comparison, in Fig. 16(a) the small strain modulus E_0, derived from V_S measured by SDMT, and the modulus E_{DMT} derived from M_{DMT}, assuming in both cases the elasticity theory and a Poisson's ratio of $\nu = 0.15$ (hence, $E_{DMT} = 0.95M_{DMT}$), are reported. Fig. 16(a) shows the progressive reduction of the back-calculated moduli E under increasing load. Such reduction should reflect the combined effects—of the opposite sign—of the increase in the stress and strain levels (the stiffness should increase with stress and decrease with the shear strain).

To separate the two effects, the dependence of E on the current stress level was taken into account, as a first approximation, by use of the Janbu's relationship

$$E = K_E p_a \left(\sigma'_v/p_a\right)^n \tag{2}$$

where K_E = modulus number; p_a = reference atmospheric pressure (100 kPa); σ'_v = current vertical effective stress; and n = exponent, generally varying between 0.5 and 1; here, assumed equal to 0.5 in accordance with Cola and Simonini (2002). The variation of modulus number K_E in Eq. (2) corresponding to E back-calculated under each load increment is represented in Fig. 16(b), which even more clearly shows the decay of stiffness, purged of the effects of stress increase, with increasing strain.

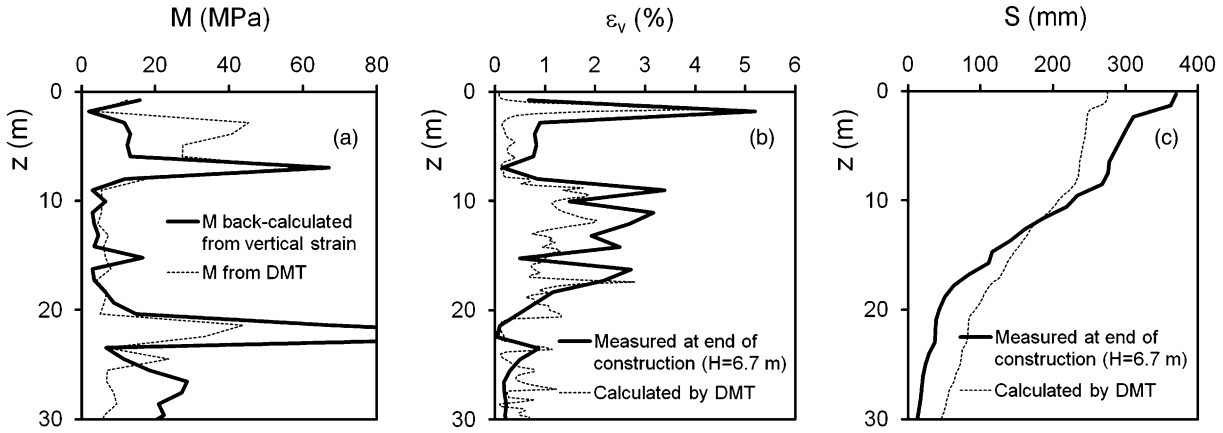

Fig. 15. Comparisons of DMT-predicted versus observed moduli and settlements under the embankment center at the end of construction: (a) M_{DMT} versus M back-calculated from local vertical strains ε_v measured by a SD at 1-m depth intervals; (b) DMT-predicted versus measured vertical strains ε_v; (c) DMT-predicted versus measured settlements S (data from Marchetti et al. 2006)

J. Geotech. Geoenviron. Eng. 2014.140:215-227.

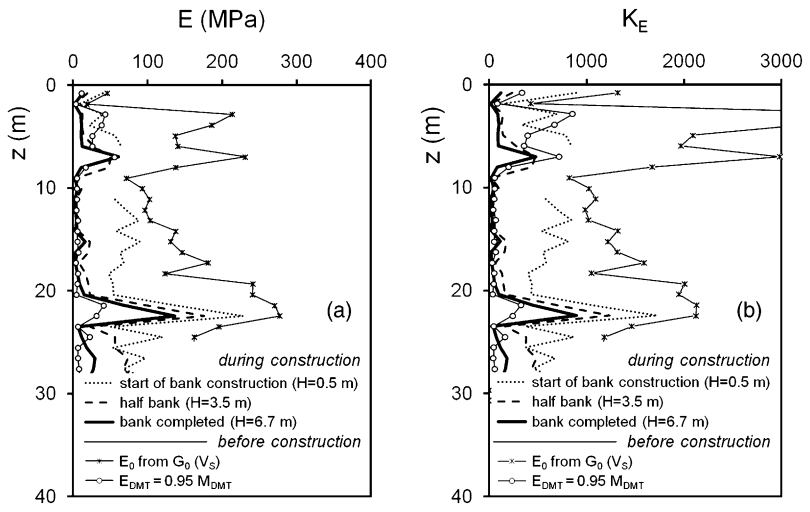

Fig. 16. Variation of (a) secant Young's modulus E and (b) corresponding modulus number K_E [Eq. (2)] back-calculated from local ε_v measured at the center under various embankment loads throughout construction (data from Marchetti et al. 2006)

In situ decay curves of soil stiffness with strain level (Fig. 17) were reconstructed from the back-calculated moduli at the midheight of each 1-m soil layer. To account for the effect of varying stress level, such in situ curves are expressed in terms of the variation of ratio K_E/K_{E0}, where K_E and K_{E0} are the modulus numbers corresponding to E back-calculated for each load increment and to initial modulus E_0, respectively [where K_{E0} is obtained by Eq. (2) for $E = E_0$ and $\sigma'_v = \sigma'_{v0}$]. The two sets of curves in Fig. 17 are representative of distinct soil layers; i.e., the sand layer between 2- and 8-m depth [Fig. 17(a)] and the silt layer between 8- and 20-m depth [Fig. 17(b)] where most of the observed settlement originated. The initial part of the curves in Fig. 17 at small strains is missing because the SDs did not provide measurements of ε_v less than $\approx 0.5-1\times10^{-2}\%$.

A research in progress, outlined by Marchetti et al. (2008), investigates the reliability of the SDMT to assess the stiffness in situ decay with strain. The proposal is to address the G-γ curves (or similar curves) in various soil types by fitting available reference typical-shape laboratory G/G_0-γ curves through two points, both obtained by the SDMT: (1) the initial small strain modulus G_0 from V_S and (2) a working strain modulus G_{DMT} corresponding to M_{DMT}. To locate the second point it is necessary to know, at least approximately, the shear strain associated with G_{DMT}. Preliminary literature indications locate the DMT moduli at an intermediate level of strain of about 0.05–0.1% (Mayne 2001) or 0.01–1% (Ishihara 2001) along the G-γ curve.

At the TTS, using the SDMT results obtained at the depth of each back-figured in situ stiffness decay curve shown in Fig. 17, Young's moduli E_{DMT} were derived from M_{DMT} by the elasticity theory (always assuming $\nu = 0.15$; hence, $E_{DMT} = 0.95M_{DMT}$) and normalized to their small strain values E_0 derived from V_S. The dots in Fig. 17 are the intersection between the in situ decay curve at a given depth and the horizontal line having as the ordinate the ratio K_E/K_{E0} corresponding to E_{DMT}/E_0 at the same depth. Such intersections provided the values of the associated abscissas; i.e., the vertical strains ε_v in this case. The rectangular shaded areas in Figs. 17(a and b) denote, for each soil layer, the range of values of the ratio K_E/K_{E0} corresponding to E_{DMT}/E_0 and the associated range of vertical strains; i.e., $\varepsilon_v \approx 0.01-0.1\%$ in sand and $\approx 0.3-1\%$ in silt. This result generally agrees with preliminary indications (Mayne 2001; Ishihara 2001).

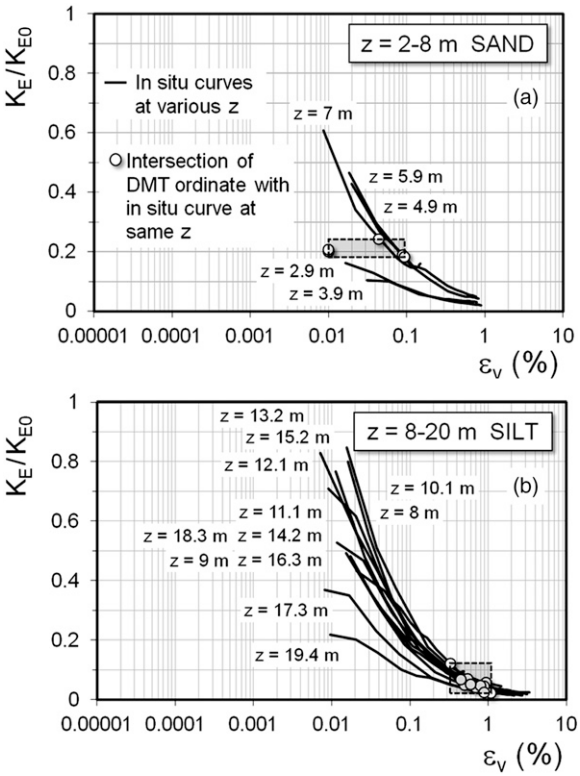

Fig. 17. Curves of soil stiffness decay with vertical strain back-calculated from local ε_v measurements (curves labeled in situ curves) (a) in the sand layer 2–8 m deep and (b) in the silt layer 8–20 m deep (the dots are the intersection between the curve at a given depth and the horizontal line having as the ordinate the ratio K_E/K_{E0} corresponding to E_{DMT}/E_0 at the same depth; such intersections provided the values of the associated abscissas ε_v) (data from Marchetti et al. 2006)

Interrelationship between Small Strain Modulus G_0 and Working Strain Modulus M_{DMT}

The interrelationship between small strain stiffness (G_0 from V_S) and working strain stiffness (M_{DMT} from the usual DMT interpretation)

J. Geotech. Geoenviron. Eng. 2014.140:215-227.

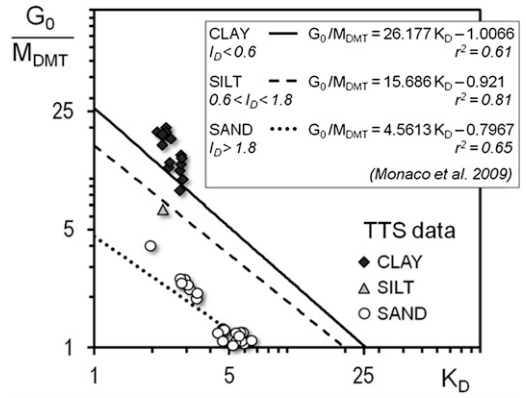

Fig. 18. Ratio G_0/M_{DMT} versus K_D (OCR) for various soil types at the TTS (data points from preconstruction and postremoval SDMT soundings 14, 19, and 20) superimposed to previously identified trends

determined by the SDMT has been investigated in previous studies (Marchetti et al. 2008; Monaco et al. 2009). These studies suggested experimental relationships of the ratio G_0/M_{DMT} as a function of the horizontal stress index K_D for three classes of soils—i.e., clay, silt and sand—constructed using 800 high-quality data points from 34 sites in a variety of soil types.

In Fig. 18 the values of the ratio G_0/M_{DMT} obtained at the TTS in SI-1 and SI-3 are plotted as a function of K_D; distinguishing among clay, silt, and sand on the basis of material index I_D. The data are superimposed to the three best-fit curves obtained by Monaco et al. (2009) for each soil type (equations indicated in Fig. 18). The following recognizable trends of the TTS data in Fig. 18 are quite similar to previous observations: (1) the data points tend to group according to their I_D (soil type); (2) G_0/M_{DMT} at the TTS is mostly in the range of 0.5–4 in sand and 8–20 in clay; (3) the maximum variability of G_0/M_{DMT} is found in clay; and (4) for all soils G_0/M_{DMT} decreases as K_D (related to the OCR) increases.

An important consideration emerging from Fig. 18 is that at the TTS, as generally observed, the ratio G_0/M_{DMT} varies in a wide range ($\approx 0.5-20$); hence, it is far from being a constant, especially in clays and silts. Its value is strongly dependent on multiple information; e.g., at least, the soil type and stress history. Therefore, it appears next to impossible to derive the operative modulus for settlement predictions from G_0 by dividing G_0 by a fixed number, as suggested by various authors.

Conclusions

The results presented in this paper have indicated the following:

1. The test embankment program provided knowledge of the OCR profiles, according to the very definition of the OCR, at two times (i.e., at full load and after load removal). These reference OCR profiles have been used to construct a correlation OCR versus M_{DMT}/q_t. Such a correlation [Eq. (1)] has been found to be in line with existing guidelines for estimating the OCR and with various previous experimental data, reinforcing the tentative hypothesis of general (although approximate) validity of such relationships. At the TTS, Eq. (1) permitted spotting unexpected higher OCR inclusions. The OCR-M_{DMT}/q_t relationship is probably also dependent, at least moderately, on D_r and the stress level. Most of the data at the base of the OCR-M_{DMT}/q_t relationships presented or referenced in this paper are for low or medium dense sands; i.e., 50 to 80%. Additional research is needed to investigate the dependency of the relationship on D_r and the stress level, and possibly on the sand type.
2. Correlations OCR versus M_{DMT}/q_t, as Eq. (1), can possibly be of help in the following two ways: (1) obtaining approximate estimates of the OCR based on the measured M_{DMT}/q_t; and (2) obtaining evaluations of the α factor for estimating the operative modulus M from the CPT as $M = \alpha q_c$, if some information is available on the stress history of the deposit. The indication from Eq. (1) would be $\alpha = 5-16$ for OCR $= 1-4.5$.
3. The observed end-of-construction settlement at the center was 38 cm. The DMT predicted settlement was 29 cm; considering that the settlement predicted by DMT is the primary settlement, while the observed 38 cm includes appreciable secondary compression during construction, the agreement appears reasonable.
4. Besides comparisons of settlements at the surface, more stringent comparisons at depths have been possible, thanks to the local vertical strain measurements provided every 1 m by the SD installed below the center. Overall satisfactory agreement has been found between the observed and DMT-predicted moduli [Fig. 15(a)]. The reference field moduli, back-figured from the in situ local strains, are disturbance free; hence, they are high-quality moduli. The observed agreement supports the assumption that M_{DMT} is a reasonable estimate of the working strain modulus; i.e., applicable to foundations under working loads.
5. Soundings performed before embankment application and postremoval have permitted comparing how the OCR caused by the embankment was reflected by the before/after SDMT and CPTU parameters. The parameter most reactive to the OCR was M_{DMT} (or K_D), the least reactive (almost insensitive to the OCR) was V_S, while q_t exhibited an intermediate reactivity.
6. A simplified attempt has been made to infer for the soil elements on the centerline the E-ε_v decay curves, and to identify in these curves the abscissa; i.e., the operative strain, to be associated to M_{DMT}, with the scope of locating the second point of the decay curve (given the first point corresponding to G_0). It was found that M_{DMT} can be possibly associated with a strain range $\varepsilon_v \approx 0.01-0.1\%$ in sand and $\approx 0.3-1\%$ in silt. Additional research in this area is considered worthwhile. In fact, determining the decay curves in the laboratory is a complex operation, while the in situ determination would be faster and operator independent.
7. Regarding the interrelationship G_0/M, the TTS G_0/M_{DMT} data points have been found in line with previously identified trends (Fig. 18). The chart permits obtaining G_0 estimates from conventional DMT data, which may be useful in cases when just the DMT data are available. An even more important indication from this chart is the impossibility, in absence of information on stress history and soil type, of obtaining the operative modulus M by dividing G_0 by a constant, considering that the range of the divisor would be $G_0/M \sim 0.5-20$.

Acknowledgments

The authors wish to extend special thanks to the Consorzio Venezia Nuova and the Magistrato alle Acque, Venezia.

References

Baldi, G., Bellotti, R., Ghionna, V. N., Jamiolkowski, M., and Lo Presti, D. C. F. (1989). "Modulus of sands from CPT's and DMT's." *Proc., 12th*

J. Geotech. Geoenviron. Eng. 2014.140:215-227.

Int. Conf. on Soil Mechanics and Foundation Engineering, Vol. 1, Balkema, Rotterdam, Netherlands, 165–170.
Cola, S., and Simonini, P. (1999). "Some remarks on the behavior of Venetian silts." *Proc., 2nd Int. Symp. on Pre-Failure Behaviour of Geomaterials*, Balkema, Rotterdam, Netherlands, 167–174.
Cola, S., and Simonini, P. (2002). "Mechanical behaviour of silty soils of the Venice lagoon as a function of their grading properties." *Can. Geotech. J.*, 39(4), 879–893.
Devincenzi, M. J., and Canicio, M. (2001). "Geotechnical characterization by in situ tests of a loess-like deposit in its natural state and after saturation." *Proc., Int. Conf. on In Situ Measurement of Soil Properties and Case Histories*, P. P. Rahardjo and T. Lunne, eds., Graduate Program, Parahyangan Catholic Univ., Bandung, Indonesia, 159–166.
Gottardi, G., and Tonni, L. (2004). "Use of piezocone tests to characterize the silty soils of the Venetian lagoon (Treporti Test Site)." *Proc., 2nd Int. Conf. on Site Characterization (ISC'2)*, Vol. 2, A. Viana da Fonseca and P. W. Mayne, eds., Millpress, Rotterdam, Netherlands, 1643–1649.
Ishihara, K. (2001). "Estimate of relative density from in-situ penetration tests." *Proc., Int. Conf. on In Situ Measurement of Soil Properties and Case Histories*, P. P. Rahardjo and T. Lunne, eds., Graduate Program, Parahyangan Catholic Univ., Bandung, Indonesia, 17–26.
Jamiolkowski, M., Ghionna, V. N., Lancellotta, R., and Pasqualini, E. (1988). "New correlations of penetration tests for design practice." *Proc., 1st Int. Symp. on Penetration Testing (ISOPT-1)*, Vol. 1, Balkema, Rotterdam, Netherlands, 263–296.
Jendeby, L. (1992). "Deep compaction by vibrowing." *Proc., Nordic Geotechnical Meeting,* Vol. 1, Danish Geotechnical Society, Lyngby, Denmark, 19–24.
Kovari, K., and Amstad, C. (1982). "A new method of measuring deformations in diaphragm walls and piles." *Geotechnique*, 22(4), 402–406.
Lee, M. J., Choi, S. K., Kim, M. T., and Lee, W. (2011). "Effect of stress history on CPT and DMT results in sand." *Eng. Geol.*, 117(3-4), 259–265.
Marchetti, S. (1980). "In situ tests by flat dilatometer." *J. Geotech. Engrg. Div.*, 106(3), 299–321.
Marchetti, S. (1985). "On the field determination of K_0 in sand." *Proc., 11th Int. Conf. on Soil Mechanics and Foundation Engineering*, Vol. 5, Balkema, Rotterdam, Netherlands, 2667–2673.
Marchetti, S. (2010). "Sensitivity of CPT and DMT to stress history and aging in sands for liquefaction assessment." *Proc., 2nd Int. Symp. on Cone Penetration Testing (CPT'10)*, P. K. Robertson and P. W. Mayne, eds., Vol. 3, Paper No. 3-50. Omnipress, Madison, WI.
Marchetti, S., Monaco, P., Calabrese, M., and Totani, G. (2004). "DMT-predicted vs measured settlements under a full-scale instrumented embankment at Treporti (Venice, Italy)." *Proc., 2nd Int. Conf. on Site Characterization (ISC'2)*, A. Viana da Fonseca and P. W. Mayne, eds., Vol. 2, Millpress, Rotterdam, Netherlands, 1511–1518.
Marchetti, S., Monaco, P., Calabrese, M., and Totani, G. (2006). "Comparison of moduli determined by DMT and backfigured from local strain measurements under a 40 m diameter circular test load in the Venice area." *Proc., 2nd Int. Conf. on the Flat Dilatometer*, R. A. Failmezger and J. B. Anderson, eds., In-Situ Soil Testing, Lancaster, VA, 220–230.
Marchetti, S., Monaco, P., Totani, G., and Calabrese, M. (2001). "The flat dilatometer test (DMT) in soil investigations—A report by the ISSMGE Committee TC16." *Proc., 2nd Int. Conf. on the Flat Dilatometer*, R. A. Failmezger and J. B. Anderson, eds., In-Situ Soil Testing, Lancaster, VA, 7–48.
Marchetti, S., Monaco, P., Totani, G., and Marchetti, D. (2008). "In situ tests by seismic dilatometer (SDMT)." *From research to practice in geotechnical engineering*, J. E. Laier, D. K. Crapps, and M. H. Hussein, eds., ASCE, Reston, VA, 292–311.
Mayne, P. W. (1991). "Tentative method for estimating σ'_{h0} from q_c data in sands." *Proc., 1st Int. Symp. on Calibration Chamber Testing*, A. B. Huang, ed., Elsevier, Potsdam, NY, 249–256.
Mayne, P. W. (2001). "Stress-strain-strength-flow parameters from enhanced in-situ tests." *Proc., Int. Conf. on In Situ Measurement of Soil Properties and Case Histories*, P. P. Rahardjo and T. Lunne, eds., Graduate Program, Parahyangan Catholic Univ., Bandung, Indonesia, 27–47.
Mayne, P. W., Coop, M. R., Springmanm, S. M., Huang, A., and Zornberg, J. G. (2009). "Geomaterial behavior and testing." *Proc., 17th Int. Conf. on Soil Mechanics and Geotechnical Engineering*, M. Hamza, M. Shahien, and Y. El-Mossallamy, eds., Vol. 4, IOS Press, Rotterdam, Netherlands, 2777–2872.
McGillivray, A., and Mayne, P. W. (2004). "Seismic piezocone and seismic flat dilatometer tests at Treporti." *Proc., 2nd Int. Conf. on Site Characterization (ISC'2)*, Vol. 2, A. Viana da Fonseca and P. W. Mayne, eds., Millpress, Rotterdam, Netherlands, 1695–1700.
Monaco, P., Marchetti, S., Totani, G., and Marchetti, D. (2009). "Interrelationship between small strain modulus G_0 and operative modulus." *Proc., Int. Conf. on Performance-Based Design in Earthquake Geotechnical Engineering*, T. Kokusho, Y. Tsukamoto, and M. Yoshimine, eds., Taylor & Francis Group, London, 1315–1323.
Monaco, P., Totani, G., and Calabrese, M. (2006). "DMT-predicted vs observed settlements: a review of the available experience." *Proc., 2nd Int. Conf. on the Flat Dilatometer*, R. A. Failmezger and J. B. Anderson, eds., In-Situ Soil Testing, Lancaster, VA, 244–252.
Schmertmann, J. H. (1983). "Revised procedure for calculating K_0 and OCR from DMT's with $I_D > 1.2$ and which incorporates the penetration force measurement to permit calculating the plane strain friction angle." *DMT Digest No. 1*, GPE Inc., Gainesville, FL.
Simonini, P. (2004). "Characterization of the Venice lagoon silts from in-situ tests and the performance of a test embankment." *Proc., 2nd Int. Conf. on Site Characterization (ISC'2)*, Vol. 1, A. Viana da Fonseca and P. W. Mayne, eds., Millpress, Rotterdam, Netherlands, 187–207.
Simonini, P., Ricceri, G., and Cola, S. (2007). "Geotechnical characterization and properties of Venice lagoon heterogeneus silts." *Proc., 2nd Int. Workshop on Characterization and Engineering Properties of Natural Soils*, Vol. 4, T. S. Tan, K. K. Phoon, D. W. Hight, and S. Leroueil, eds., Taylor & Francis Group, London, 2289–2328.
Tonni, L., and Gottardi, G. (2011). "Analysis and interpretation of piezocone data on the silty soils of the Venetian lagoon (Treporti test site)." *Can. Geotech. J.*, 48(4), 616–633.
Tonni, L., Gottardi, G., Berengo, V., and Simonini, P. (2010). "Classification, overconsolidation and stiffness of Venice lagoon soils from CPTU." *Proc., 2nd Int. Symp. on Cone Penetration Testing (CPT'10)*, P. K. Robertson and P. W. Mayne, eds., Vol. 2, Omnipress, Madison, WI.
Yamashita, S., Jamiolkowski, M., and Lo Presti, D. (2000). "Stiffness nonlinearity of three sands." *J. Geotech. Geoenviron. Eng.*, 126(10), 929–938.